Energy transport and light propagation mechanisms in organic single crystals

Bernd Wittmann, Stephan Wiesneth, Sajedeh Motamen, Laurent Simon, Françoise Serein-Spirau, Günter Reiter, Richard Hildner

Energy transport and light propagation mechanisms in organic single crystals

Bernd Wittmann[1], Stephan Wiesneth[1], Sajedeh Motamen[2], Laurent Simon[3],

Françoise Serein-Spirau[4], Günter Reiter[2], Richard Hildner*[1,5]

[1]Spectroscopy of Soft Matter, University of Bayreuth, Universitätsstraße 30, 95447 Bayreuth, Germany.

[2]Institute of Physics, University of Freiburg, Hermann-Herder-Straße 3, 79104 Freiburg, Germany.

[3]Institut de Sciences des Materiaux de Mulhouse IS2M, LRC 7228-CNRS-UHA, 4 rue des freres Lumiere, 68093 Mulhouse, France

[4] Institut Charles Gerhardt de Montpellier, UMR 5353-CNRS Equipe Architectures Moleculaires et Materiaux Nanostructures (AM2N), Ecole Nationale Superieure de Chimie de Montpellier, 8 Rue de l'Ecole Normale, 34296 Montpellier cedex 05, France

[5]Zernike Institute for Advanced Materials, University of Groningen, Nijenborgh 4, 9747 AG Groningen, The Netherlands.

*Correspondence to: r.m.hildner@rug.nl.

Abstract:

Unambiguous information about spatio-temporal exciton dynamics in three-dimensional nano- to micrometre-sized organic structures is difficult to obtain experimentally. Exciton dynamics can be modified by annihilation processes, and different light propagation mechanisms can take place, such as active waveguiding and photon recycling. Since these various processes and mechanisms can lead to similar spectroscopic and microscopic signatures on comparable time scales, their discrimination is highly demanding. Here, we study individual organic single crystals grown from thiophene-based oligomers. We use time-resolved detection-beam scanning microscopy to excite a local exciton population and monitor the subsequent broadening of the photoluminescence (PL) signal in space and on pico- to nanosecond time scales. Combined with Monte Carlo simulations we were able to exclude photon recycling for our system, whereas leakage radiation upon active waveguiding leads to an apparent PL broadening of about 20% compared to the initial exciton profile. Exciton-exciton annihilation becomes important at high excitation fluence and apparently accelerates the exciton dynamics leading to apparently increased diffusion lengths. At low excitation fluences the spatio-temporal PL broadening results from exciton diffusion with diffusion lengths of up to 210 nm. Surprisingly, even in structurally highly ordered single crystals, the transport dynamics is subdiffusive and shows variations between different crystals, which we relate to varying degrees of static and dynamic electronic disorder.

Introduction:

Transport of excitation energy in assemblies of functional organic molecules is a key process in e.g. organic solar cells and organic light-emitting diodes [1–4]. In particular, the exciton diffusion length, i.e., the distance over which energy can be transported, is of great importance for device efficiency [2–4]: While in solar cells a long transport distance is desired to reach an interface for generation of free charge carriers, in light-emitting diodes long transport distances can lead to unwanted non-radiative quenching at defect sites. Precise measurements of transport distances and dynamics are therefore required to be able to understand energy transport properties and to ultimately optimize molecular assemblies for the desired functionality.

Currently, organic single crystals attract substantial attention as suitable building blocks for new devices and applications [1,5–13]. In structurally highly ordered crystals molecules are densely packed and thus feature reasonably strong electronic Coulomb interactions. Hence, delocalised singlet exciton states form in which electronic excitations are coherently shared by many molecules (coherent transport). However, unavoidable electronic and structural disorder leads to a localisation of excitons. In particular, at room temperature dephasing processes due to interaction with the local environment occur on typical timescales of some 100 fs and rapidly attenuate coherent transport by dynamically localising exciton wave functions. On pico- to nanosecond time scales, relevant in the context of this work, energy transport then takes place as incoherent hops between (more or less) delocalized exciton states [14–18]. To resolve these complex energy transport processes direct measurements of transport distances and diffusivities in single crystals would be ideal, yet, those are scarce and demanding. For too high excitation densities such measurements can easily be misleading, since several excitons within the exciton diffusion length can be created. Excitons can then

interact and annihilate (**Fig. 1a**), which yields an apparent increase in diffusion lengths and prevents a precise characterisation of energy transport distances [19–21]. A further complication arises, because organic crystals are three-dimensional systems with spatial dimensions of some tens of nanometres up to millimetres, and they possess usually a higher refractive index than their surrounding media. In this situation, different light propagation mechanisms can occur upon photoexcitation: First, active waveguiding can take place (**Fig. 1b**). Photoluminescence (PL) emitted within a crystal is reflected at interfaces of the crystal with e.g. a substrate or air. A fraction of light remains confined within the structure and propagates over long (µm to mm) distances [5,6,22]. Notably, we have recently demonstrated that an organic layer with a sub-wavelength thickness of ca. 50 nm supports already active waveguiding [23]. In addition to such propagating waveguide modes, so-called radiative leaky waveguide modes (**Fig. 1b**) leave the structure into the substrate in close proximity to the excitation position [24], which can erroneously be attributed to energy transport. Second, photon recycling can take place, which refers to re-absorption and re-emission of photons by other (distant) molecules within a crystal (**Fig. 1c**). This effect can be significant if the PL quantum yield is high and/or the absorption and PL spectra strongly overlap [25,26]. Since all these processes (except waveguiding) often occur on similar time scales, their discrimination and quantification become very challenging. The unambiguous identification of these processes, however, is of key importance to extract correct exciton diffusion lengths and to develop suitable design principles for novel structures.

To study energy transport in molecular assemblies, various indirect methods have been applied to date [27], such as time-resolved exciton-exciton annihilation [16], and PL quenching at sensitisers or surfaces [2,28–30]. However, these methods have several shortcomings: They are usually applied to large ensembles (films and solutions) and

thus average over disorder. Annihilation measurements on bulk samples lack *direct* spatial information, i.e., we do not know where the annihilation process takes place. Finally, quencher molecules or nearby surfaces perturb the system by deliberately introducing defects. Only a few direct measurements of transport distances have been reported. These techniques exploit that an initial, spatially defined exciton population broadens in space due to energy transport. A simple approach uses static microscopy to create an initial exciton population in a defined spatial region, e.g., by a diffraction-limited excitation spot. The spatial broadening is detected by PL imaging and ananlysed by comparing this PL image with the initial exciton population [31–35]. Using confocal microscopy with time-resolved detection-beam scanning [36,37], the spatial broadening of the PL signal can be followed on pico- to nanosecond time scales. The time resolution can be extended to the femtosecond range with transient absorption microscopy [19,38,39]. The temporal information of these direct methods allows to rule out waveguiding via leaky modes as broadening effect, since waveguiding occurs quasi instantaneously with the speed of light. But the distinction between exciton transport, annihilation and photon recycling requires a more careful design of experiments and data evaluation.

Here, we report on the quantification of the spatio-temporal dynamics of energy transport, annihilation and light propagation mechanisms in organic single crystals based on thiophene-benzene-thiophene (3TBT) oligomers (see **Fig. S1**) [22,40]. These crystals are grown as previously described and possess a well-defined elongated geometry with the 3TBT oligomers being stacked cofacially along the long axis (*y* direction, **Fig. 1d**) [22]. This H-type assembly of 3TBT molecules should favour long-range transport of excitation energy (singlet excitons) along the crystals' long axis [32], which, however, has not been detected so far. The crystals' µm-scale dimensions and high refractive index allow for efficient active waveguiding [22,24]. Moreover, the spectral

overlap between the absorption and PL spectra enables photon recycling. To distinguish the different transport regimes and propagation mechanisms, we use confocal PL microscopy combined with detection-beam scanning and time-correlated single-photon counting, see Supporting Information (Materials and Methods). In combination with Monte-Carlo simulations, we are able to distinguish and quantify all transport/propagation mechanisms. We find that exciton diffusion represents the dominant contribution to the broadening of the diffraction-limited excitation spot in 3TBT crystals on a pico- to nanosecond timescale, while waveguiding via radiative leaky modes and photon recycling play only a minor role. Despite subdiffusive exciton transport in our highly ordered crystals, we observe long energy transport lengths up to 210 nm.

Results:

A widefield PL image of a representative 3TBT crystal with a width of 2.7 µm and a length exceeding 30 µm is shown in **Fig. 2a**. The crystal shows a weak and relatively homogeneous PL from its body and bright emission from its tip. This behaviour is characteristic of active waveguiding of PL that is emitted within the crystal into propagating waveguide modes and out-coupled at the crystal tip [22,24].

Upon confocal excitation of the crystal at the position labelled with the green filled circle in **Fig. 2b**, we observe two distinct emission spots: First, there is relatively weak emission from the crystal tip (red dashed box), which results from active waveguiding of PL created at the excitation spot. Second, we observe direct emission from the excitation position (blue dashed box), which is clearly broadened along the crystal's long (y-) axis compared to the excitation profile (**Fig. 2c** and **Fig. S2**). We recently

attributed this broadening to result predominantly from short-distance (μm) leaky-mode active waveguiding into the substrate [24]. However, based on the highly ordered H-type arrangement of the 3TBT molecules with reasonable electronic Coulomb coupling of about 320 cm^{-1} [13], substantial exciton diffusion lengths are to be expected as well. Moreover, 3TBT crystals feature strong spectral overlap between the absorption and PL spectra with a substantial extinction coefficient of ~0.2 μm^{-1} (**Fig. S3** and Ref. [24]), which, in principle, enables photon recycling. Hence, there is a clear need to discriminate between these transport/propagation mechanisms.

Photon recycling. We first address photon recycling by measuring PL lifetimes at different positions, while the excitation remains fixed at the position labelled with the green filled circle in **Fig. 2b**. We recorded the PL lifetimes from this excitation position (blue dashed box) as well as from the crystal tip (red dashed box), which is 14 µm away from the excitation. The PL decay curves from both positions are identical and show a lifetime of $\tau = 0.35ns$ (**Fig. 2d**, see **Fig. S4** for a second example). Photon recycling would lead to increasingly longer PL lifetimes with increasing distance to the excitation spot [25,26] due to delayed emission of (re-)absorbed and re-emitted photons. Thus, we can rule out photon recycling as a significant propagation mechanism over 14 µm towards the crystal tip. Since the probability for photon re-absorption (and thus re-emission) follows the Lambert-Beer law, photon recycling can not dominate the PL broadening on a much smaller length scale below 1 µm directly around the excitation spot (**Fig. 2c**). To further corroborate this finding, we simulated photon recycling using a kinetic Monte-Carlo ray tracing algorithm (**Fig. S5**). We indeed found only a very small fraction of photons (< 3.4%) that is recycled over a distance of 14 µm (**Figs. S6-S8**, **Tab. S1**). We can thus exclude photon recycling for our system.

Leaky-mode waveguiding. To quantify the contribution of leakage radiation into the substrate in the vicinity of the excitation spot upon short-distance (µm) waveguiding, we performed a detection beam scanning experiment on the crystal shown in **Fig. 2**. We kept the excitation position fixed and measured PL decay curves, while scanning the detection position across the excitation position by some µm along the long crystal axis. To avoid exciton-exciton annihilation, we used a low excitation fluence of 0.4 µJ/cm² and thus created only about 2.4 excitations/µm along one π–stack of 3TBT molecules. **Fig. 3a** shows the resulting normalised PL intensity distribution, $I(y,t)$, as a function of distance *y* relative to the centre of the excitation spot (*y*=0) and time *t* after laser excitation. This distribution reveals a slight broadening of the PL signal along the crystal's long axis within one nanosecond.

Considering the timescale of this broadening, this cannot result from leakage radiation. The latter propagates with the speed of light and can thus only affect the smallest observable, instantaneous width of the PL profile at t=0, but does not account for further spatio-temporal dynamics. Indeed, the instantaneous PL profile $I(y,t=0)$ has a rather broad full width at half maximum (FWHM) of about 760 nm **(Fig. S9)**. Measuring the influence of leakage radiation on this instantaneous PL profile requires two reference samples: A very thin sample and one with the same dimensions as the crystal in **Fig. 2a** with identical refractive index, surface roughness, etc., but without the ability of exciton diffusion. Such reference samples, however, are very difficult to realise. Thus, we demonstrate the instantaneous broadening due to radiative leaky-mode waveguiding using a Monte-Carlo ray trace algorithm that simulates PL profiles at the excitation position for two crystals with different heights (**Fig. S10**): One has a height of 2 µm, which is similar to that in the experiment and features waveguiding; the second crystal has a height of only 5 nm, and thus waveguiding and radiative leaky modes are suppressed. Note that photon recycling was 'deactivated' in these

simulations by setting the PL quantum yield to zero (see SI). We find that the FWHM of the PL profile at $t = 0$ is 20% broader for the thick crystal compared to the thin one (**Fig. S10**). This effect is exclusively caused by the µm dimensions of the thick crystal with accompanying leakage radiation upon waveguiding.

Exciton Diffusion. The pico- to nanosecond broadening of the PL intensity distribution $I(y,t)$ in **Fig. 3a** is attributed to exciton diffusion over many tens of nanometres [20,36,37]. That is, the initial exciton population, created by the excitation pulse, is transported away from the excitation spot prior to (radiative) decay. We analysed the time-dependent broadening of this $I(y,t)$ distribution by calculating the mean-square displacement (MSD) as a function of time. We used a reconvolution approach to account for all instantaneous non-Gaussian broadening effects due to e.g. leaky-mode waveguiding (see SI for details). The measured spatio-temporal PL distribution $I(y,t)$ is fitted by a convolution of the initial (non-Gaussian) profile $I(y,t=0)$ and the Gaussian probability density function for exciton diffusion $G(y,t)$:

$$I(y,t) = I(y,0) * G(y,t). \qquad (1)$$

The Gaussian function $G(y,t)$ results from the solution of the (time-dependent) diffusion equation (see SI, section "Incoherent exciton diffusion model"), and the variance of $G(y,t)$ corresponds to the MSD reflecting the PL broadening due to transport as a function of time. The evolution of the MSD for the data in **Fig. 3a** is shown in **Fig. 3c** (red points). We observe a clear sub-linear behaviour, which is characteristic of subdiffusive exciton motion. This indicates the presence of static and dynamic disorder that increasingly slows down diffusion for longer times [10,14,41,42]. We found the same qualitative behaviour for 14 other single crystals (**Fig. S11**).

Subdiffusive motion can be modelled by fitting the MSD with a 1-dimensional model [14,41,43,44]:

$$MSD(t) = At^{\alpha}. \qquad (2)$$

Here α is the diffusion exponent and A is the exciton hopping coefficient, which is related to a time-dependent diffusivity via $D(t) = \frac{1}{2}A_{\alpha}t^{\alpha-1}$. For normal diffusion, α=1, the diffusivity becomes time independent. In contrast, for subdiffusive motion, α<1, a time-dependent diffusivity $D(t)$ arises, which results from a disordered energy landscape with asymmetric hopping rates (see Fig. 1a). Both the exponent and time-dependent diffusivity are determined by a fit to the data (**Fig. 3c**, red points, solid line). The exponent is $\alpha = 0.59 \pm 0.03$, which indicates subdiffusion. The analysis of in total 14 different crystals yields a distribution of diffusion exponents with a mean value of $\bar{\alpha} = 0.70 \pm 0.23$ (**Fig. S11**). This variability of the exponent for different crystals is remarkable, since these are usually considered to be highly defined. Our observation thus underpins the intrinsic heterogeneous nature of organic self-assembled materials [36,37]. The time-dependent diffusivity determined from the fit **(Fig. 3d**, red line) exhibits a rapid decrease by more than one order of magnitude within the first nanosecond. The initial high diffusivity is probably caused by fast relaxation between and within the vibronic exciton bands to lower energy exciton states [14,41,45–47]and a subsequent equilibration into a quasi-static diffusion within the inhomogeneously broadened excited-state energy landscape of the crystal. Moreover, fast (sub-)picosecond fluctuations of electronic interaction between molecules, induced by low-energy phonon modes of the crystal, can contribute to rapid coherent transport in this initial time window of our measurement [48,49]. Using the excited-state lifetime $\tau = 0.35\ ns$ (**Fig. 3e**, red), measured for this low-fluence excitation, we find here $D(\tau) = 0.19\ cm^2/s$ (see also **Fig. S11**).

The analysis of the MSD as a function of time also allows us to retrieve the exciton diffusion length in this system using the square root of the maximum MSD, $L_D =$

$\sqrt{\max(MSD(t))}$. From the measurement shown in **Fig. 3a** we find a diffusion length of $0.19\ \mu m$. For the measurements on 14 crystals, we find that the diffusion lengths are distributed around an average value of $\bar{L}_D = 0.17 \pm 0.02\ \mu m$, and a maximum diffusion length of 0.21 µm (**Fig. S11**). These exciton diffusion lengths are among the largest reported for H-aggregated crystalline structures [28,29,39].

Exciton-exciton annihilation. To characterize the influence of increasing excitation fluence, and thus of exciton-exciton annihilation on the PL intensity distributions, we conducted an additional detection-beam scanning measurement at a high fluence of 40 µJ/cm², corresponding to 240 excitations/µm (**Fig. 3b**). Notably, this measurement was performed on the same crystal and at the same excitation position as that shown in **Fig. 3a**. The presence of annihilation in our data is verified by the reduction of the excited-state lifetime from $\tau = 0.35\ ns$ at low fluence to $\tau = 0.28\ ns$ at high fluence (**Fig. 3e**). Laser excitation generates an initial density of excitons within the excitation spot, which can diffuse as well as decay radiatively and non-radiatively. Interaction between excitons leads to annihilation, and thus to an additional decay channel with a concomitant decrease in the PL-lifetime. **Fig. 3b** shows the normalized spatial PL intensity distribution from the detection-beam scanning experiment at high fluence. Compared to the low-fluence measurement, the intensity distribution broadens faster and in a more pronounced way over the entire time range.

Following the same approach for the analysis of the PL broadening as above, we find that the MSDs are systematically larger for each point in time as compared to the low fluence experiment (**Fig. 3c**, black dots *vs.* red dots). At high fluence the subdiffusive behaviour is still clearly visible. Based on the 1-dimensional diffusion model, we find a smaller diffusion exponent of $\alpha = 0.44 \pm 0.02$, and a larger diffusivity, which steeply decreases as function of time (**Fig. 3d**, black line). At the excited state lifetime $\tau =$

$0.28ns$ under high fluence excitation (**Fig. 3e**, black), we find $D(\tau) = 0.67\ cm^2/s$. Moreover, the exciton diffusion length increases to L_D= 270 nm, which, however, is only an apparent increase. At higher fluence the mobility seems to be enhanced (larger $D(\tau)$), but diffusion is increasingly hindered by annihilation (smaller α). Importantly, this behaviour is not included in standard rate equation approaches for normal diffusion commonly applied to model such data [50,51], see also **Fig. S12**.

To gain insight into the relationship between energetic disorder, annihilation as well as the spatio-temporal dynamics of exciton diffusion, we performed kinetic Monte-Carlo simulations (see SI for details). For these simulations we averaged over 2000 energy landscapes with random Gaussian energy disorder. The same realisations of energy landscapes were used for both excitation densities of 2.4 excitations/μm and 240 excitations/μm as in the experiment. Our simulations in **Fig. 4a-d** reproduce all experimental trends, i.e., a time-dependent broadening of the exciton distribution as well as an apparently enhanced exciton mobility (and decreased diffusion exponent) for high excitation densities. Notably, we were only able to reproduce our data, in particular the high diffusion lengths in the subdiffusive regime, under the assumption of incoherent hops of delocalised excitons. In other words, a combined coherent-incoherent transport of excitons takes place, and a purely incoherent hopping from site to site is not sufficient to model our data (see SI, Kinetic Monte Carlo Simulation of Exciton-Exciton Annihilation, for details).

The apparent enhancement of the diffusivity at high excitation fluence can be traced back to the spatio-temporal behaviour of the annihilation probability: The Gaussian excitation profile creates an initial Gaussian-shaped exciton population. The loss of excitations due to annihilation is therefore highest in the centre of this distribution [19] and at short times after laser excitation (**Fig. S13**). As illustrated in **Fig. 4e**, at early times we find an annihilation probability of 96% for high fluence (while for low fluence

it is only 22 %). Consequently, in the high fluence regime annihilation rapidly thins out the exciton population in the centre of the initial distribution. In other words, the peak exciton population is rapidly reduced, which 'cuts off' the peak of the PL-intensity profile at short times and artificially broadens this initial PL profile in space. The annihilation probability then decreases with time (**Fig. 4e**) due to annihilation, exciton diffusion and (non-)radiative decay. Exciton diffusion spatially broadens the annihilation probability with time (**Fig. S13**), which causes the PL intensity distribution to broaden further. This spatio-temporal behaviour of the annihilation probability highlights the efficiency of energy transport in our 3TBT crystals. Our simulations along with our experiments thus reveal the origin of the apparently changed singlet exciton dynamics for increasing excitation fluences.

Conclusion:

We studied the spatio-temporal dynamics of energy transport and light propagation mechanisms in micrometre-scale 3TBT-based organic single crystals as a model system. We focussed here specifically on transport/propagation processes along the long axis of the crystals, which corresponds to the π-stacking direction of the 3TBT molecules. Along this direction the Coulomb interaction between molecules is strongest and thus (long-range) singlet exciton transport is most efficient. We used detection-beam scanning methods in combination with kinetic Monte-Carlo simulations to distinguish between photon recycling, radiative leaky-mode waveguiding, energy transport and exciton-exciton annihilation. We excluded photon recycling as the main effect of the broadened emission in 3TBT crystals, because it only accounts for 3.4% of all detected photons. However, our study illustrates that photon recycling can be significant in organic structures with a high PL quantum yield and large overlap between the PL and absorption spectra, which is typical for J-aggregates. Moreover,

our simulations show that photon recycling is manifested in spatio-temporal data with very similar characteristics as exciton diffusion. Leaky-mode waveguiding leads to about 20% instantaneous broadening of the non-Gaussian emission profile at time t=0 of the spatio-temporal PL-intensity distributions. If not taken into account, this mechanism therefore leads to a substantial overestimation of the total exciton diffusion lengths determined by steady-state direct imaging methods.

Only the pico- to nanosecond temporal broadening of the spatial PL intensity distribution in the 3TBT crystals can be unambiguously attributed to exciton diffusion, if low excitation fluences are used to avoid annihilation. Under those conditions, we found surprisingly large exciton diffusion lengths up to 210 nm, which we related to combined coherent-incoherent transport, i.e., incoherent hopping of delocalised exciton states. Exciton-exciton annihilation results in an apparent broadening of the spatial PL-intensity distribution with increasing excitation fluence, and thus leads to an overestimation of exciton diffusion lengths. Independent of the excitation fluence, the temporal PL-broadening exhibits a clear subdiffusive behaviour during the entire time-range. This observation is in contrast to standard rate equation approaches [19,50] that assume normal diffusion for the short-time dynamics and a transition to subdiffusive transport at later times. In general, subdiffusive behaviour results from intrinsic disorder in organic structures. Since the structural arrangement of molecules, especially in single crystals, is very well-defined, this disorder is very likely purely electronic in nature and comprises both static and dynamic contributions. For instance, the degree of side group crystallinity can vary locally, which spatially modulates excited-state energy levels by providing locally slightly different (static) dielectric environments for each 3TBT molecule. This effect has been shown to be relevant for e.g. P3HT aggregates [52]. Fast fluctuations of (groups of) side chains or vibrations, such as (acoustic) phonon modes, contribute to dynamic electronic disorder. On the one hand,

these fluctuations shift energy levels on fast time scales [14,53] (usually sub-picoseconds at room temperature) via a time-dependent local dielectric environment. On the other hand, these can induce fluctuations of the electronic coupling by modulating inter-molecular distances [42,48,49]. Therefore, a deep understanding of all parameters that dictate exciton transport must be obtained, which requires unambiguous resolution of exciton dynamics in molecular assemblies. Our results highlight that quantification of spatio-temporal exciton dynamics in nano- to micrometre scale organic structures requires careful evaluation of different energy transport regimes and light propagation mechanisms.

Supplementary Material:

See Supplementary Material for a description of materials and methods, of control experiments, of kinetic Monte Carlo ray tracing simulations of photon recycling and leaky mode waveguiding, and of kinetic Monte Carlo simulations of exciton transport and annihilation.

Acknowledgements:

We acknowledge financial support from the German Research Foundation (DFG) through project GRK1640 (BW and RH) and IRTG1642 (GR), stimulating discussions with Christian Schörner, and the continued support of this work by Jürgen Köhler.

Data Availability Statement:

The data that support the findings of this study are available from the corresponding author upon reasonable request.

References and Notes:

[1] C. Zhang, Y. Yan, Y.S. Zhao, and J. Yao, Acc. Chem. Res. **47**, 3448 (2014).

[2] S.M. Menke and R.J. Holmes, Energy Environ. Sci. **7**, 499 (2014).

[3] O. V. Mikhnenko, P.W.M. Blom, and T.Q. Nguyen, Energy Environ. Sci. **8**, 1867 (2015).

[4] H. Paul, C. David, and B.P. Rand, Acc. Chem. Res. **42**, 1740 (2009).

[5] Q.H. Cui, Q. Peng, Y. Luo, Y. Jiang, Y. Yan, C. Wei, Z. Shuai, C. Sun, J. Yao, and Y.S. Zhao, Sci. Adv. **4**, 1 (2018).

[6] M.P. Zhuo, J.J. Wu, X.D. Wang, Y.C. Tao, Y. Yuan, and L.S. Liao, Nat. Commun. **10**, 1 (2019).

[7] L. Zang, Acc. Chem. Res. **48**, 2705 (2015).

[8] M.J. Sun, Y. Liu, Y. Yan, R. Li, Q. Shi, Y.S. Zhao, Y.W. Zhong, and J. Yao, J. Am. Chem. Soc. **140**, 4269 (2018).

[9] G.B. Piland and C.J. Bardeen, J. Phys. Chem. Lett. **6**, 1841 (2015).

[10] C.J. Bardeen, Annu. Rev. Phys. Chem. **65**, 127 (2014).

[11] J. Gierschner and S.Y. Park, J. Mater. Chem. C **1**, 5818 (2013).

[12] J. Gierschner, L. Lüer, B. Milián-Medina, D. Oelkrug, and H.J. Egelhaaf, J. Phys. Chem. Lett. **4**, 2686 (2013).

[13] S. Motamen, D. Raithel, R. Hildner, K. Rahimi, T. Jarrosson, F. Serein-Spirau, L. Simon, and G. Reiter, ACS Photonics **3**, 2315 (2016).

[14] S.M. Vlaming, V.A. Malyshev, A. Eisfeld, and J. Knoester, J. Chem. Phys. **138**, 214316 (2013).

[15] J.M. Moix, M. Khasin, and J. Cao, New J. Phys. **15**, 085010 (2013).

[16] J.R. Caram, S. Doria, D.M. Eisele, F.S. Freyria, T.S. Sinclair, P. Rebentrost, S. Lloyd, and M.G. Bawendi, Nano Lett. **16**, 6808 (2016).

[17] J.L. Brédas, E.H. Sargent, and G.D. Scholes, Nat. Mater. **16**, 35 (2016).

[18] F. Fassioli, R. Dinshaw, P.C.C. Arpin, and G.D.D. Scholes, J. R. Soc. Interface **11**, 20130901 (2014).

[19] T. Zhu, Y. Wan, and L. Huang, Acc. Chem. Res. **50**, 1725 (2017).

[20] N.S. Ginsberg and W.A. Tisdale, Annu. Rev. Phys. Chem. **71**, 1 (2020).

[21] E.M. Grumstrup, Opt. Express **27**, 31385 (2019).

[22] S. Motamen, C. Schörner, D. Raithel, J.P. Malval, T. Jarrosson, F. Serein-Spirau, L. Simon, R. Hildner, and G. Reiter, Phys. Chem. Chem. Phys. **19**, 15980 (2017).

[23] C. Schörner, C. Neuber, and R. Hildner, APL Photonics **4**, (2019).

[24] C. Schörner, S. Motamen, L. Simon, G. Reiter, and R. Hildner, ACS Omega **3**, 6728 (2018).

[25] Y. Fang, H. Wei, Q. Dong, and J. Huang, Nat. Commun. **8**, (2017).

[26] I. Dursun, Y. Zheng, T. Guo, M. De Bastiani, B. Turedi, L. Sinatra, M.A. Haque, B. Sun, A.A. Zhumekenov, M.I. Saidaminov, F.P. García De Arquer, E.H. Sargent, T. Wu, Y.N. Gartstein, O.M. Bakr, O.F. Mohammed, and A. V. Malko, ACS Energy Lett. **3**, 1492 (2018).

[27] J.D.A. Lin, O. V. Mikhnenko, J. Chen, Z. Masri, A. Ruseckas, A. Mikhailovsky, R.P. Raab, J. Liu, P.W.M. Blom, M.A. Loi, C.J. García-Cervera, I.D.W. Samuel, and T.Q. Nguyen, Mater. Horizons **1**, 280 (2014).

[28] A.K. Topczak, T. Roller, B. Engels, W. Brütting, and J. Pflaum, Phys. Rev. B **89**, 201203 (2014).

[29] X.H.H. Jin, M.B.B. Price, J.R.R. Finnegan, C.E.E. Boott, J.M.M. Richter, A. Rao, S. Matthew Menke, R.H.H. Friend, G.R.R. Whittell, and I. Manners, Science (80-.). **360**, 897 (2018).

[30] A.A. Mannanov, M.S. Kazantsev, A.D. Kuimov, V.G. Konstantinov, D.I. Dominskiy, V.A. Trukhanov, D.S. Anisimov, N. V Gultikov, V. V Bruevich, I.P. Koskin, A.A. Sonina, T. V Rybalova, I.K. Shundrina, E.A. Mostovich, D.Y. Paraschuk, and M.S. Pshenichnikov, J. Mater. Chem. C **7**, 60 (2019).

[31] K.A. Clark, E.L. Krueger, and D.A. Vanden Bout, J. Phys. Chem. Lett. **5**, 2274 (2014).

[32] A.T. Haedler, K. Kreger, A. Issac, B. Wittmann, M. Kivala, N. Hammer, J. Köhler, H.W. Schmidt, and R. Hildner, Nature **523**, 196 (2015).

[33] P. Irkhin and I. Biaggio, Phys. Rev. Lett. **107**, 17402 (2011).

[34] P. Avakian and R.E. Merrifield, Phys. Rev. Lett. **13**, 541 (1964).

[35] K. Narushima, S. Hirata, and M. Vacha, Nanoscale **9**, 10653 (2017).

[36] G.M. Akselrod, P.B. Deotare, N.J. Thompson, J. Lee, W.A. Tisdale, M.A. Baldo, V.M. Menon, and V. Bulovic, Nat. Commun. **5**, 3646 (2014).

[37] B. Wittmann, F.A. Wenzel, S. Wiesneth, A.T. Haedler, M. Drechsler, K. Kreger, J. Köhler, E.W. Meijer, H.-W. Schmidt, and R. Hildner, J. Am. Chem. Soc. **142**, 8323 (2020).

[38] C. Schnedermann, J. Sung, R. Pandya, S.D. Verma, R.Y.S. Chen, N. Gauriot, H.M. Bretscher, P. Kukura, and A. Rao, J. Phys. Chem. Lett. **10**, 6727 (2019).

[39] R. Pandya, R.Y.S. Chen, Q. Gu, J. Gorman, F. Auras, J. Sung, R. Friend, P. Kukura, C. Schnedermann, and A. Rao, J. Phys. Chem. A **124**, 2721 (2020).

[40] R.A. Silva, F. Serein-Spirau, M. Bouachrine, J.P. Lère-Porte, and J.J.E. Moreau, J. Mater. Chem. **14**, 3043 (2004).

[41] G.M. Akselrod, F. Prins, L. V. Poulikakos, E.M.Y. Lee, M.C. Weidman, A.J. Mork, A.P. Willard, V. Bulović, and W.A. Tisdale, Nano Lett. **14**, 3556 (2014).

[42] R.P. Fornari, J. Aragó, and A. Troisi, J. Phys. Chem. C **120**, 7987 (2016).

[43] J. Wu and K.M. Berland, Biophys. J. **95**, 2049 (2008).

[44] S. Havlin and D. Ben-Avraham, Adv. Phys. **51**, 187 (2002).

[45] R. Kersting, U. Lemmer, R.F. Mahrt, K. Leo, H. Kurz, H. Bässler, and E.O. Göbel, Phys. Rev. Lett. **70**, 3820 (1993).

[46] R. Hildner, U. Lemmer, U. Scherf, and J. Köhler, Chem. Phys. Lett. **429**, 103 (2006).

[47] G.R. Hayes, I.D.W. Samuel, and R.T. Phillips, Phys. Rev. B **52**, 569 (1995).

[48] J. Aragó and A. Troisi, Phys. Rev. Lett. **114**, 26402 (2015).

[49] J. Aragó and A. Troisi, Adv. Funct. Mater. **26**, 2316 (2016).

[50] S. Deng, E. Shi, L. Yuan, L. Jin, L. Dou, and L. Huang, Nat. Commun. **11**, 1 (2020).

[51] Y. Wan, Z. Guo, T. Zhu, S. Yan, J. Johnson, and L. Huang, Nat. Chem. **7**, 785 (2015).

[52] F. Panzer, M. Sommer, H. Bässler, M. Thelakkat, and A. Köhler, Macromolecules **48**, 1543 (2015).

[53] R. Hildner, L. Winterling, U. Lemmer, U. Scherf, and J. Köhler, ChemPhysChem **10**, 2524 (2009).

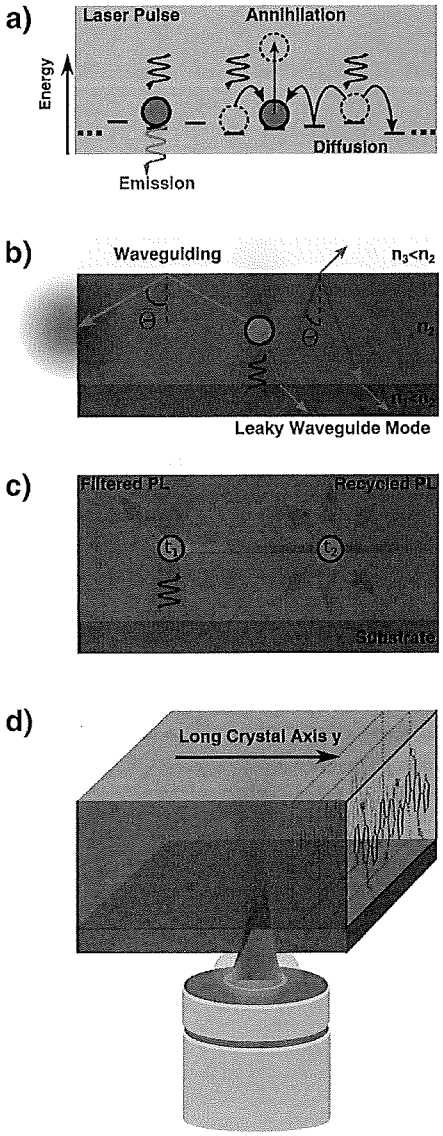

Figure 1. Energy transport and light propagation mechanisms in organic single crystals. **(a)** Exciton diffusion in a disordered energy landscapePhotogenerated excitons can diffuse, annihilate or (radiatively) decay. . Horizontal lines represent segments over which excitons (red circles) can be delocalized; the thick black arrows indicate (incoherent and coherent) transport of excitons. **(b)** Active waveguiding of photoluminescence created within the crystal: The crystal, with anisotropic refractive index n_2, is surrounded by media with lower refractive indices (glass substrate: n_1, air: n_3). If emitted light is reflected at an angle $\bar{\Theta}$ larger than the critical angle for total internal reflection, it is guided towards the crystal tip and then out-coupled. For angles Θ smaller than the critical angle the emitted light can escape into the surrounding media (radiative leaky waveguide modes). **(c)** Photon recycling: PL generated at time $t=t_1$ is re-absorbed during its propagation through the crystal, which can generate delayed emission at $t_2>t_1$. **(d)** Schematic illustration of the detection-beam scanning PL measurements on a 3TBT crystal: The crystal is confocally excited at a fixed position (light blue), while the detection position (red) is independently moved along the crystal's long (y-) axis.

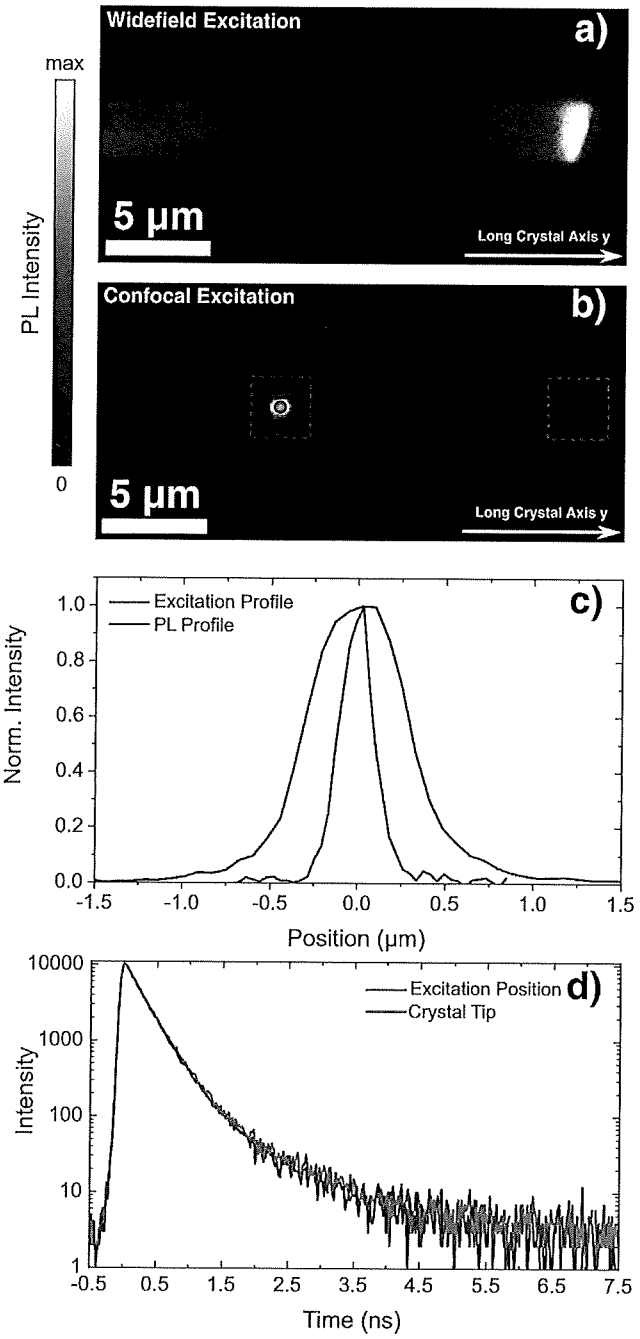

Figure 2. **(a)** Widefield PL image of a 3TBT single crystal. **(b)** PL image of the same crystal upon confocal excitation at the position marked with the green filled circle (within the blue dashed box). The blue and red dashed boxes indicate the detection area for PL decay measurements. **(c)** Excitation (green) and PL emission profile (blue) retrieved at the excitation position within the blue square in (b) along the long crystal axis. **(d)** PL decay curves measured for a spatially fixed excitation (green circle in (b)) at the excitation position (blue) and at the tip of the crystal (red) after light propagation.

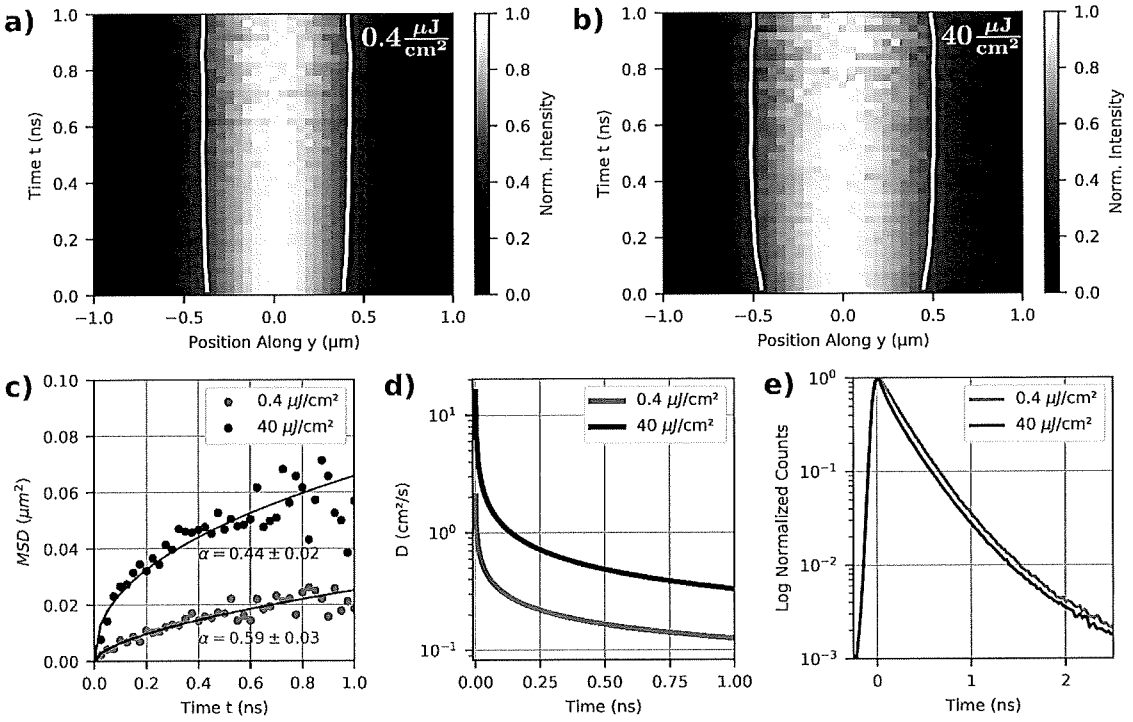

Figure 3. **(a, b)** Normalized PL intensity distributions *I(y,t)* and their spatio-temporal evolution for the 3TBT crystal in Fig. 2, measured along the long crystal axis for an excitation fluence of 0.4 μJ/cm² (a) and 40 μJ/cm² (b). The white contour lines indicate the time evolution of the full width at half maximum. Note that around t = 1 ns the PL signal is already quite small so that the profiles appear to become narrower again. **(c)** Temporal changes of the mean square displacements (MSD) calculated from a (red) and b (black). The solid lines represent fits to a power law with a diffusion exponent α. **(d)** Time-dependent diffusivities *D(t)*, as determined from the fits to the MDS curves in c. **(e)** PL lifetime curves determined from the distributions in a (red) and b (black) by spatial integration.

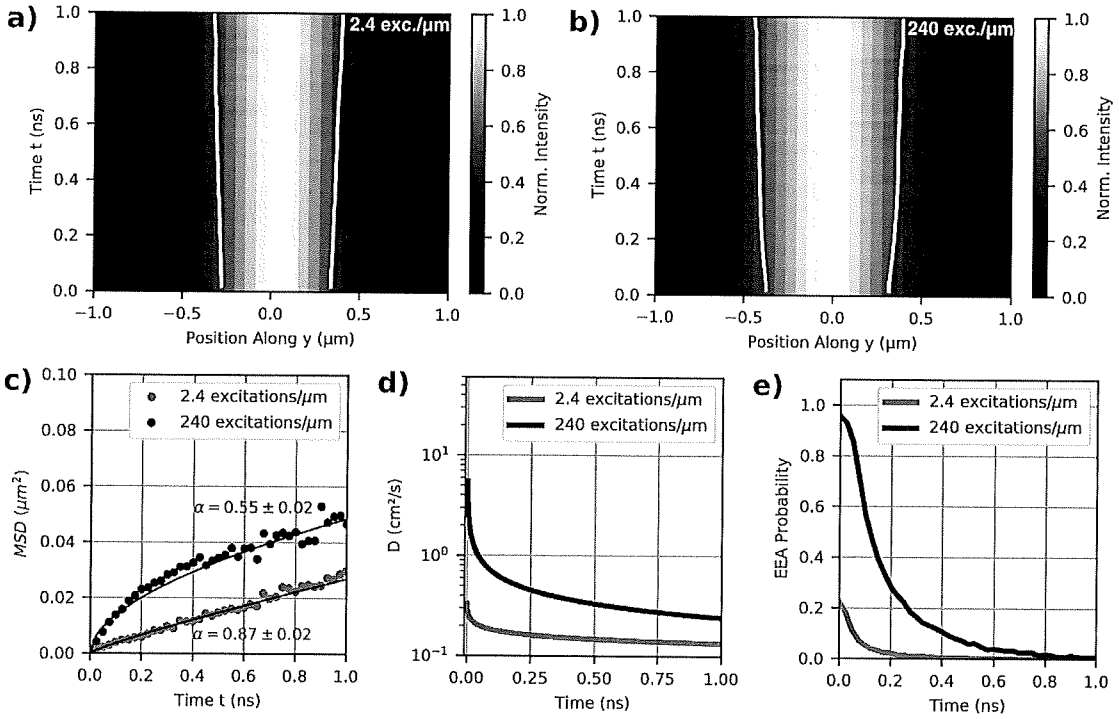

Figure 4. Kinetic Monte Carlo simulations of exciton diffusion and exciton-exciton annihilation. **(a, b)** Simulated normalized PL intensity distributions and their spatio-temporal evolution for an average over 2000 realizations of energetic disorder. The initial excitation densities were 2.4 excitations/µm (a) and 240 excitations/µm (b). The white contour lines indicate the time evolution of the full width at half maximum. **(c)** Temporal changes of the simulated MSD (dots) from a and b, with power law fits (solid lines). **(d)** Time-dependent diffusivities *D(t)*. **(e)** Calculated probabilities for exciton-exciton annihilation as a function of time.